Model calculation of production rates, ion and electron densities in the evening troposphere of Mars at latitudes 67°N and 62°S: Seasonal variability

S. A. Haider,[1] Varun Sheel,[1] V. Singh,[2] W. C. Maguire,[3] and G. J. Molina-Cuberos[4]

Received 7 December 2007; revised 19 March 2008; accepted 23 April 2008; published 28 August 2008.

[1] We have developed a model to calculate the production rates and densities of positive and negative ions in the troposphere of Mars at evening. Using this model, the densities of 35 ions (A_r^+, O_2^+, CO_2^+, $O_2^+CO_2$, NO^+, H_3O^+, $H_3O^+H_2O$, $H_3O^+(H_2O)_2$, $H_3O^+(H_2O)_3$, $H_3O^+(H_2O)_4$, H_3O^+HO, $CO_2^+CO_2$, CO^+, C^+, N_2^+, NO^+CO_2, N^+, $O_2^+(CO_2)_2$, $O_2^+H_2O$, $O_2^+(H_2O)_2$, O_4^+, O^+, $CO_3^-H_2O$, $CO_3^-(H_2O)_2$, CO_3^-, CO_4^-, NO_2^-, $NO_2^-H_2O$, $NO_2^-(H_2O)_2$, NO_3^-, $NO_3^-H_2O$, $NO_3^-(H_2O)_2$, O_2^-, O_3^-, O^-) are estimated in summer and winter at latitudes 67°N and 62°S for solar zenith angles 80° and 85°, respectively. The impact ionization source is taken as galactic cosmic rays. The model atmospheres at these locations are constructed from air density measured by radio occultation experiment aboard Mars Global Surveyor. The maximum electron densities in southern winter and northern summer are obtained at altitudes ~25 km and ~30 km, respectively, due to high efficiency of electron attachment to O_x molecules. Of the 35 ions considered in the model, the chemistry of 9 major ions ($H_3O^+(H_2O)_n$ for n = 1, 2, 3, 4 and CO_4^-, CO_3^-, $NO_2^-H_2O$ and $CO_3^-(H_2O)_n$ for n = 1, 2) are discussed in this paper. The ion densities are changed by factors of 5 to 10 between these two seasons.

Citation: Haider, S. A., V. Sheel, V. Singh, W. C. Maguire, and G. J. Molina-Cuberos (2008), Model calculation of production rates, ion and electron densities in the evening troposphere of Mars at latitudes 67°N and 62°S: Seasonal variability, *J. Geophys. Res.*, *113*, A08320, doi:10.1029/2007JA012980.

1. Introduction

[2] The Radio occultation experiment onboard Mars Global Surveyor (MGS) contributes detailed measurements to an improved understanding of the basic thermal structure, circulation, and dynamics of the troposphere of Mars. These results are based on analysis of the radio signal received from MGS as it enters and exits occultation by the planet. Occultation studies with MGS encompass a range of diverse phenomena that has been investigated based on high vertical resolution profiles of atmospheric density, pressure, and temperature [*Tyler et al.*, 2001]. These measurements are made available by radio science team at NASA's Planetary Data System (http:/pds-geophys.wustl.edu/pds/mgs/rs/).

[3] In this paper we have used temperature and air density profiles measured by radio occultation experiment at solar zenith angles 85° and 80° on 3 March and 30 December 1998 for Ls = 285° and 67° in southern and northern hemispheres, respectively, at nearly same latitude and longitude (62°S, 205°E; 67°N, 200°E). At the time of these measurements, Mars had winter in south and summer in north with moderate solar activity period ($f_{10.7}$ = 132–181). Two model atmospheres of 12 gases (CO_2, N_2, A_r, O_2, H_2, CO, H_2O, O, O_3, NO, NO_2, and HNO_3) are obtained at these locations from measured air density by multiplying it by the mixing ratio of their gases [*Rodrigo et al.*,1990; *Nair et al.*, 1994; *Tyler et al.*, 2001]. We have examined the seasonal variability in the calculation of ion production rates and electron density. The model calculations are carried out between altitudes 1 to 40 km at observed points. The ion production rates are calculated because of the impact of galactic cosmic rays by using the energy loss method which is described in section 3. The production rate and temperature have been used later in the continuity equation for the calculation of ion and electron densities under photochemical steady state condition.

[4] The first theoretical study of the Martian lower ionosphere was carried out by *Whitten et al.* [1971]. They considered the ionization by cosmic rays and solar radiation in the dayside ionosphere of Mars. Later *Molina-Cuberos et al.* [2002] calculated electron density in the nighttime lower ionosphere of Mars. Recently *Haider et al.* [2007] have estimated mean electron density in the nighttime ionosphere of Mars due to absorption of solar wind electron and galactic cosmic rays between altitudes 0 and 220 km.

[1]Department of Space and Atmospheric Sciences, Physical Research Laboratory, Ahmedabad, India.
[2]Department of Electronics for Automation, Faculty of Engineering, Universita' degli Studi di Brescia, Brescia, Italia.
[3]Solar System Exploration Division, NASA Goddard Space Flight Centre, Greenbelt, Maryland, USA.
[4]Depto. Fisica, Faculted Quimica, Universidad de Murcia, Murcia, Spain.

Copyright 2008 by the American Geophysical Union.
0148-0227/08/2007JA012980

These authors did not study the lower atmosphere/ionosphere of Mars at daytime. In this region, the ion neutral chemistry is similar to the D region of Earth's ionosphere, which is formed because of the following ionization sources: (1) solar Lyman α (1216 Å) ionizing the minor constituent NO, (2) solar X-ray ($\lambda < 8$ Å) ionizing N_2 and O_2, (3) cosmic ray ionizing all atmospheric constituents and (4) photoionization of the metastable $O_2(^1\Delta_g)$ by solar UV radiation ($\lambda < 1118$ Å). We have found earlier that maximum ionization occurs in the dayside Martian ionosphere at altitudes ~125 km and ~105 km due to absorption of solar EUV (≤1025.7 Å) and X-ray photons (≤90 Å), respectively [*Haider et al.*, 2002]. The ionization due to Lyman α (1216 Å) is not studied in the lower ionosphere of Mars. This source plays active role in the mesosphere of Earth. The cosmic ray ionization is found an important process in the lower atmosphere of Mars at nighttime [*Molina-Cuberos et al.*, 2002; *Haider et al.*, 2007].

[5] The objective of this paper is to calculate production rate, ion and electron densities in the evening due to precipitation of galactic cosmic rays in Marian troposphere at high northern and southern latitudes during summer and winter seasons, respectively. This calculation suggests that the hydrated hydronium ions $H_3O^+(H_2O)_{2,3}$ and water cluster ions $NO_2^-H_2O$ and $CO_3^-(H_2O)_{1,2}$ are dominant in the Martian troposphere. The densities of these ions are changed by factors of 5 to 10 between the two seasons. The maximum electron densities in southern winter and northern summer are obtained at altitudes ~25 km and ~30 km with the concentrations of ~70 cm^{-3} and ~80 cm^{-3}, respectively, because of the high efficiency of electron attachment to O_x molecules. The concentrations of negative ions are higher than that of electron below 25 km.

[6] It is generally accepted that global electric circuit is driven by thunderstorms. The cloud and dust particle have been observed in the troposphere of Mars [*Montmessin et al.*, 2006]. Thunderstorm and lightning are formed on earth by charging of clouds. The electrical conductivity is not observed in the Martian troposphere. However such charging would occur within the clouds observed on Mars. We have calculated densities of positive ions, negative ions, and electrons in the troposphere of Mars. Attachment of these particles to dust is an important loss process for the atmospheric electricity [*Michael et al.*, 2007]. In absence of conductivity measurement at Mars, this calculation can be used as a diagnostic tool for future design of electrical payloads and for the subsequent data analysis to confirm the presence of lightning in the Marian troposphere.

2. Composition of the Martian Atmosphere: An Overview

[7] In the first observation of the Martian atmosphere, *Kuiper* [1952] has inferred carbon dioxide abundance ~ 4.4 × 10^5 Dobson (Dobson ≡ 10^{-3} cm-amagat). *Grandjean and Goody* [1955] pointed out that this amount of Martian CO_2 was dependent on Kuiper's implicit assumption a surface pressure close to one-half the sea level pressure on earth. After several years, *Spinrad et al.* [1963] discovered the presence of water vapor inferring a column abundance of 10 μm. Soon after *Kaplan et al.* [1964] reported a pressure independent evaluation of the CO_2 abundance of 55 ± 20 × 10^5 Dobson and derived Martian surface pressure ~ 25 ± 15 mb. These conclusions were greatly strengthened by determination of the total pressure ~ 4.1–6.0 mb from the Mariner 4 spacecraft [*Kliore et al.*, 1965]. Since 80 × 10^5 Dobson of CO_2 would produce a surface pressure of 6 mb on Mars, it appeared likely that at least 90% of the atmosphere consisted of this gas.

[8] Carbon monoxide was first detected in the 2–0 band near 2.5 μm by *Kaplan et al.* [1969], who deduced CO abundance of 5.6 × 10^3 Dobson. These observations were also carried out by *Young and Young* [1977], who had reported same result ~5.6 ± 0.5 × 10^3 Dobson. The amount of atomic hydrogen at ~250 km was deduced to be 3 × 10^4 atoms/cm^3 [*Anderson and Hord*, 1971].Atomic oxygen at 135 km was estimated to lie between 0.5 and 1% of the total density at that altitude [*Strickland et al.*, 1972]. After many unsuccessful attempts, molecular oxygen was finally detected by *Barker* [1972] and by *Carleton and Traub* [1972] as 9.0 ± 0.6 × 10^3 Dobson and 10.4 ± 1.0 × 10^3 Dobson, respectively.

[9] Ozone was discovered by *Barth and Hord* [1971] from observations with UV spectrometer onboard Mariner 7 spacecraft. Abundance less than 3 × 10^{-1} Dobson were recorded over most of the planet, while values ranging from 3 × 10^{-1} to 60 × 10^{-1} Dobson were found over the cold polar caps [*Barth et al.*, 1973]. An upper limit of 0.5 to 5% of N_2 was reported from Mariner 6 and 7 measurements [*Dalgarno and McElroy*, 1970]. Mars 6 measurements seemed to indicate that as much as 35% of the atmosphere might be a noble gas [*Istomin and Grechnev*, 1976]. Finally, Viking Lander verified the presence of nitrogen and argon [*Nier et al.*, 1976; *Owen and Biemann*, 1976]. The molecular oxygen, carbon monoxide, and atomic oxygen were also confirmed in the Martian atmosphere. Subsequent analysis and data from the second Viking Lander added nitric oxide, krypton, xenon, and neon to the list of species in the Martian atmosphere [*Nier et al.*, 1976; *Biemann et al.*, 1976; *Owen et al.*, 1976; *McElroy et al.*, 1976; *Owen et al.*, 1977].

[10] Modeling has provided a better knowledge of the neutral compositions and structure compared to what was known earlier. *Rodrigo et al.* [1990] and *Nair et al.* [1994] have modeled the atmospheric constituents CO_2, N_2, A_r, O_2, CO, H_2O, H_2, O, O_3, NO, NO_2, and HNO_3. *Molina-Cuberos et al.* [2002] have used this model atmosphere to study nighttime lower ionosphere of Mars. We have used mixing ratios of these gases in the construction of model atmospheres of two different seasons at high northern and southern latitudes. Same mixing ratios are taken in both model atmospheres. Variation in mixing ratios can vary neutral density of minor constituents. The concentrations of major gases are not much affected because of the change in mixing ratios. Additional refinement of meteorological models and further calibration of mass spectrometer data may be expected to change the mixing ratios somewhat in both hemispheres. Although it will require additional in situ analysis of the Martian atmosphere to bring about substantial improvements. Figures 2a and 2b represent the derived neutral density profiles for summer and winter seasons at latitudes 67°N and 62°S, respectively. The neutral densities

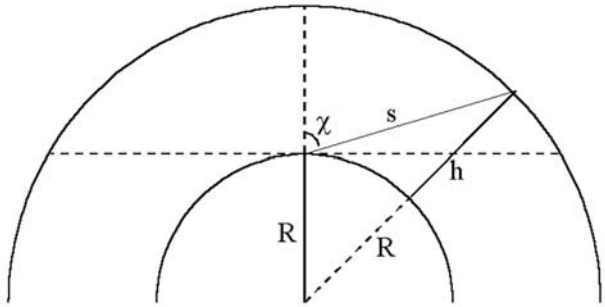

Figure 1. Schematic diagram for cosmic ray absorption in the Martian troposphere at solar zenith angle χ.

are larger in northern summer by a factor of ~2 than that of southern winter.

3. Energy Loss Model

[11] The high energy cosmic rays pass through the atmosphere, producing nucleonic cascades. The impact of primary cosmic rays, mainly protons and α particle onto the atmospheric molecules produces protons, neutrons, and pions. Fast secondary nucleons can gain enough energy to increase the production of particles by neutral collisions. Neutral pions quickly decay to gamma rays, and their contribution to the energy deposition is very important in the lower part of the atmosphere. At high altitude the maximum ion production rates are due to protons. Charged pions decay to muons, which do not decay before reaching the ground, and hence the muon energy is mainly transferred to the surface.

[12] The atmospheric thickness of Mars is defined as [*Turunen et al.*, 1996]:

$$X = \int_s^\infty \rho \ ds \tag{1}$$

where ρ is the mass density along slant paths as shown in Figure 1. Assuming a spherical atmosphere, whose density falls exponentially with increasing radius, the atmospheric depth becomes

$$X = \rho_o \int_s^\infty \exp(-h/h_o) ds \tag{2}$$

From ideal gas law, $\rho_o = X_o/h_o$, where h_0 is the scale height equal to 11 km, X_0 (= 20 gm/cm^2) is the total atmospheric depth of Mars in the vertical direction and h is height which can be represented as:

$$h = s\cos\chi + s^2/2R \tag{3}$$

Using equations (1), (2), and (3) we can calculate atmospheric thickness in troposphere of Mars as given below:

$$X(s,\chi) = \frac{X_0}{h_0} \int_s^\infty \exp\left[-\left(s^2/2R + s.\cos\chi\right)/h_0\right] ds \tag{4}$$

where R is the radius of Mars equal to 3390 km and χ is the zenith angle. The value of term $s^2/2R$ is insignificant for χ up to ~85°, therefore we can use the approximation as:

$$X(s,\chi) = \frac{X_0}{\cos\chi} \exp(-s.\cos\chi/h_0) \tag{5}$$

[13] The differential flux of the particles generated by galactic cosmic rays at depth X is given by *O'Brien et al.* [1996] as:

$$F_j(X,E) = \langle B_j \rangle \frac{X}{\lambda} e^{-X/\Lambda} \frac{L_0}{E^{\gamma+1}\left(1+u_j\right)} \tag{6}$$

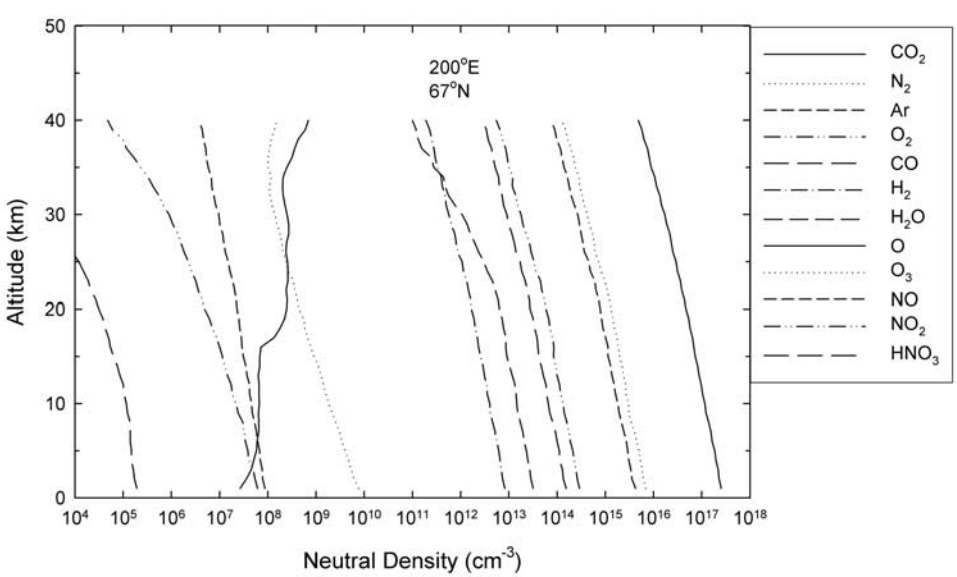

Figure 2a. Neutral densities of Martian troposphere at latitude 67°N and longitude 200°E for solar zenith angle 80°.

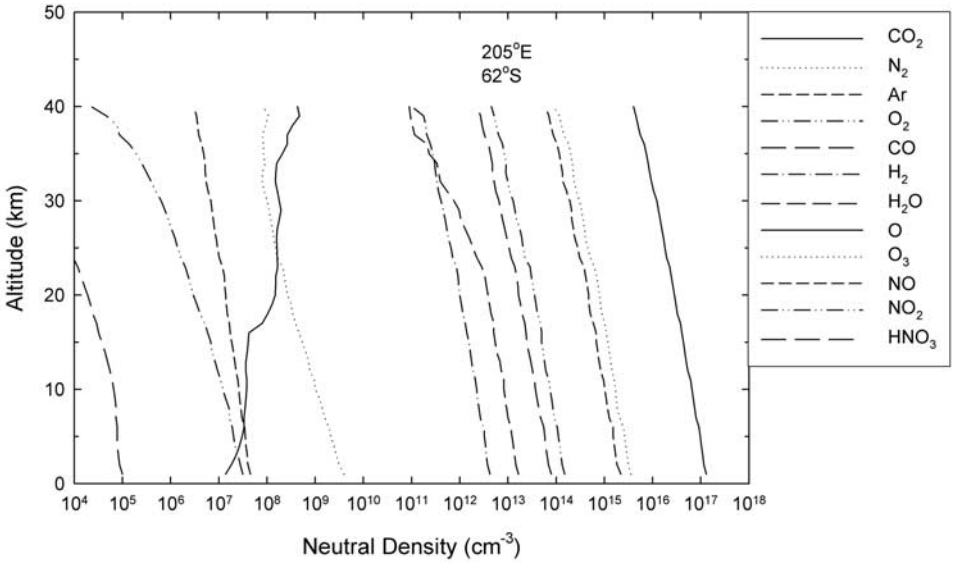

Figure 2b. Neutral densities of Martian troposphere at latitude 62°S and longitude 205°E at solar zenith angle 85°.

$$u_j = \frac{Hm_j}{c\tau_j E} \tag{7}$$

$$\langle B_j \rangle = \int_0^1 n_j(r_j).r_j.dr_j \tag{8}$$

where E is the energy, $\frac{L_0}{E^{\gamma+1}}$ is the cosmic ray nucleon spectrum at the top of the atmosphere, Λ and λ are the attenuation and interaction mean free path of the nucleon, respectively, m_j and τ_j are the mass and life time of the particle j, H is the scale height of the atmosphere, $n_j(r_j)$ is the number of particles of type j, which receive a fraction r_j of the incident nucleon energy in an interaction. In order to derive equation (6), it is assumed that interaction mean free paths of pions and kaons are equal to Λ. The value of L_0 is taken to be 2.35×10^4, if the flux is measured in m^{-2} s^{-1} $ster^1$ GeV^1. γ is equal to 1.67. The interaction and attenuation mean free path of nucleons are equal to 75 gm/cm^2 and 120 gm/cm^2, respectively.

[14] The energy loss per cm path into the material media by a particle traveling with the velocity V and undergoing inelastic collisions is written as [cf. *Evans*, 1955; *Haider et al.*, 2007]:

$$\left(\frac{dE}{dh}\right)_{ion} = \frac{2\pi e^4}{m_0 V^2} NZ \left\{ \ln\left[\frac{m_0 V^2 E}{I^2(1-\beta^2)}\right] - \beta^2 \right\} \text{ergs/cm} \tag{9}$$

[15] For simplicity, it is convenient to introduce $m_0V^2 = \beta^2 m_0 c^2$ and $E + m_0c^2 = m_0c^2/\sqrt{1-\beta^2}$ thus obtaining from equation (9)

$$\left(\frac{dE}{dh}\right)_{ion} = 4\pi r_0^2 \frac{m_0 c^2}{\beta^2} NZ \left\{ \ln\beta\left(\frac{E+m_0c^2}{I}\right)\left(\frac{E}{m_0c^2}\right)^{\frac{1}{2}} - \frac{1}{2}\beta^2 \right\} \text{MeV/cm} \tag{10}$$

where E is the energy, I is ionization potential, N is the neutral density r_0 is classical electron radius with $4\pi r_0^2 = 1.00 \times 10^{-24}$ cm^2/electron; $\beta^2 = (V/c)^2 = 1 - [(E/m_0c^2)+1]^{-2}$, $m_0c^2 = 0.51$ MeV (rest energy of electron), Z is the atomic number and c is the velocity of light.

[16] Using equation (10) the ion production rate at height h and solar zenith angle χ is given below:

$$p(h,\chi) = \frac{1}{Q}\int_E \int_\Omega (dE/dh)\ F\ (\chi, E, \Omega) d\Omega dE \tag{11}$$

where Q = 35 eV is the energy required for the formation of an electron ion pair, χ are taken as 80° and 85°, F is the total differential flux of the galactic cosmic rays being expressed in cm^{-2} s^{-1} GeV^{-1} ster^{-1} at height h and Ω is the spatial angle. Since the cosmic rays penetrate isotropically into the atmosphere, equation (11) reduces as follows:

$$p(h,\chi) = \frac{2\pi}{Q}\int (dE/dh) F(\chi, E) dE \tag{12}$$

[17] The ion density is calculated from the continuity equations neglecting transport as follows:

$$\frac{dn_i}{dt} = q_i - n_i l_i \tag{13}$$

where q_i and l_i are the total production rate (because of cosmic ray ionization and chemical reactions) and loss rate coefficient of *i*th gas, respectively. n_i is the ion density. The time dependent chemical production and loss rates of a general reaction $A^+ + B \rightarrow C^+ + D$ are given below:

$$\frac{dq_{C^+}}{dt} = R[A^+][B] \tag{14}$$

$$\frac{dl_{A^+}}{dt} = R[A^+][B] \tag{15}$$

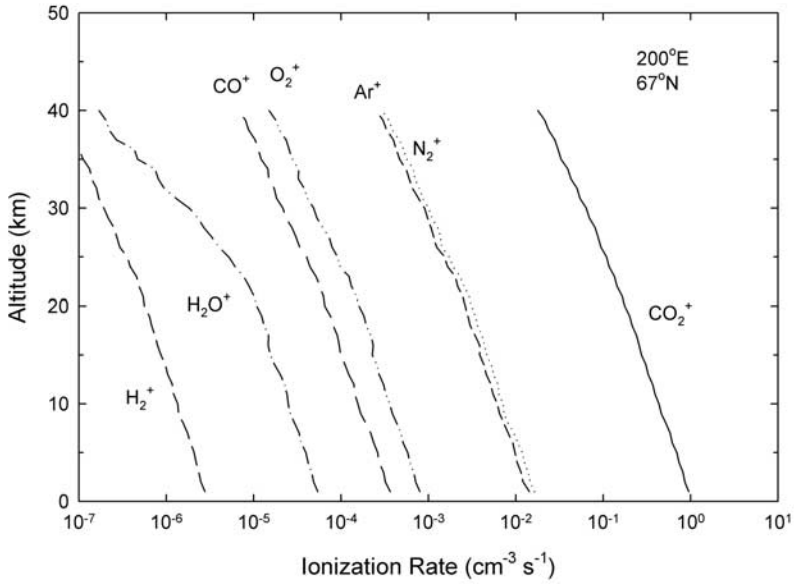

Figure 3a. Model calculation of ion production rates of CO_2^+, N_2^+, Ar^+, O_2^+, CO^+, H_2O^+, and H_2^+ at latitude 67°N and longitude 200°E for solar zenith angle 80°.

[18] In this reaction ion C^+ is produced and A^+ is lost at same chemical rate coefficient R. Under steady state condition, $\frac{dn_i}{dt} = 0$. Using equations (13), (14), and (15) the concentration of positive ion n_i^+, negative ion n_i^-, and electron n_e are calculated by iteration process as given below:

$$n_i^+ = \frac{P^i + \sum_{k,j} R^i_{k,j} n_k n_j^+ + \sum_j \gamma^i_j n_j^+}{\sum_k K^i_k n_k + \alpha^i_e n_e + \alpha_{ii} n^- + \Gamma^i} \tag{16}$$

$$n_i^- = \frac{\sum_j A^i_j n_j n_e + \sum_{k,j} R^i_{k,j} n_k n_j^- + \sum_j \gamma^i_j n_j^-}{\sum_k K^i_k n_k + \alpha_{ii} n^- + \Gamma^i} \tag{17}$$

$$n_e = \frac{\sum_j P^j + \sum_j \gamma^e_j n_j^-}{\sum_j B_j n_j + \sum_j \alpha^i_e n_i^+} \tag{18}$$

$$n^+ = n^- + n_e \tag{19}$$

$$n^+ = \sum_i n_i^+ \tag{20}$$

$$n^- = \sum_i n_i^- \tag{21}$$

where Pi is the production rate of positive ion i by galactic cosmic rays; $R^i_{k,j}$ is the rate coefficient of the reaction of neutral k with ion j to produce the ion i; γ^i_j is the rate coefficient of production of ion i by photon collision with ion j; K^i_j the rate coefficient of the reaction to remove ions i by reaction with neutral k; α^i_e and α_{ii} are the ion-electron and ion-ion recombination rate coefficient; n^+ and n^- are the total density of positive and negative ions; Γ^i is the coefficient rate of loss of ion i by photon collision; A^i_j is the rate coefficient of the production of negative ion i by electron attachment to neutral k; γ^e_j is the rate coefficient of electron production by photodetachment of ion j; and Bj is the attachment of electron to molecule nj.

4. Results and Discussions

[19] In Figures 3a and 3b, we represent production rates of major ions (CO_2^+, N_2^+, Ar^+, O_2^+, CO^+, H_2O^+, and H_2^+) at high northern and southern latitudes for summer and winter seasons, respectively. The production rates of O^+, O_3^+, NO^+, NO_2^+, and HNO_3^+ are very low, therefore they are not plotted in these figures. These production rates are used in the calculation of the densities of 35 ions viz. A_r^+, O_2^+, CO_2^+, $O_2^+CO_2$, NO^+, H_3O^+, $H_3O^+H_2O$, $H_3O^+(H_2O)_2$, $H_3O^+(H_2O)_3$, $H_3O^+(H_2O)_4$, H_3O^+HO, $CO_2^+CO_2$, CO^+, C^+, N_2^+, NO^+CO_2, N^+, $O_2^+(CO_2)_2$, $O_2^+H_2O$, $O_2^+(H_2O)_2$, O_4^+, O^+, $CO_3^-H_2O$, $CO_3^-(H_2O)_2$, CO_3^-, CO_4^-, NO_2^-, $NO_2^-H_2O$, $NO_2^-(H_2O)_2$, NO_3^-, $NO_3^-H_2O$, $NO_3^-(H_2O)_2$, O_2^-, O_3^-, O^-.

[20] The number densities of five major positive ions ($H_3O^+(H_2O)_n$ for n = 1, 2, 3, 4) and H_3O^+ are shown in Figures 4a and 4b at latitudes 67°N and 62°S during summer and winter seasons, respectively. The ions CO_2^+ and O_2^+ are produced initially because of the impact of galactic cosmic rays with the lower atmosphere of Mars. Later nearly 100% $O_2^+CO_2$ is formed because of the three body reaction, which is fully destroyed by water vapor in the formation of H_3O^+ as:

(R1) $$O_2 + CR \rightarrow O_2^+$$

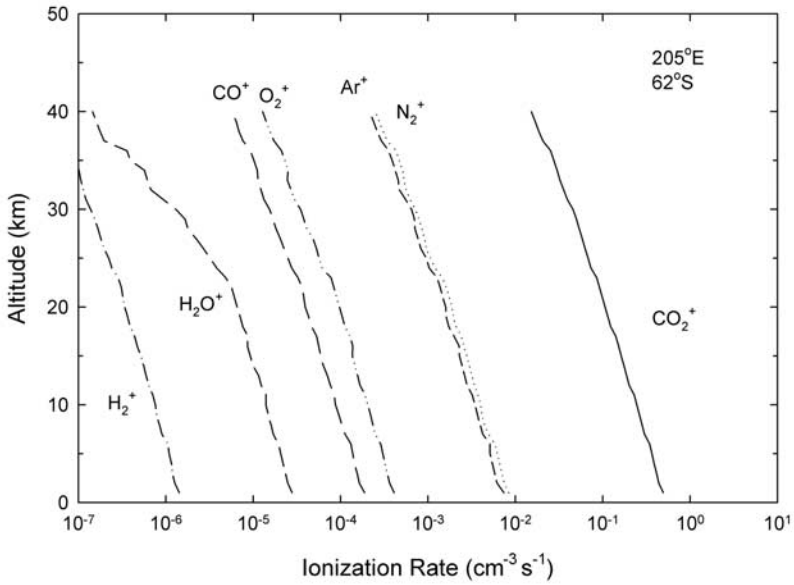

Figure 3b. Model calculation of ion production rates of CO_2^+, N_2^+, Ar^+, O_2^+, CO^+, H_2O^+, and H_2^+ at latitude 62°S and longitude 205°E for solar zenith angle 85°.

(R2) $$CO_2 + CR \rightarrow CO_2^+$$

(R3) $$O_2^+ + CO_2 + M \rightarrow O_2^+CO_2 + M$$

(R4) $$O_2^+CO_2 + H_2O \rightarrow O_2^+H_2O + CO_2$$

(R5) $$O_2^+H_2O + H_2O \rightarrow H_3O^+ + HO + O_2$$

The ion H_3O^+ is lost by three body reaction in the formation of hydrated ions $H_3O^+(H_2O)_n$ for n = 1, 2, 3, and 4. Once H_3O^+ ion has been produced water vapor molecules are associated into it. We have considered the reactions of production and loss to form cluster ions up to four water molecules as:

(R6) $$H_3O^+(H_2O)_n + H_2O + M \leftrightarrow H_3O^+(H_2O)_{n+1} + M$$

These reactions are important for the formation of hydrated ions in the troposphere of Mars. The dissociative recombination of $H_2O^+(H_2O)_n$ are always smaller than any other loss process in the troposphere.

[21] The nighttime ionosphere of Mars has been observed above the surface of Mars from Mars 4 and Mars 5 on 10

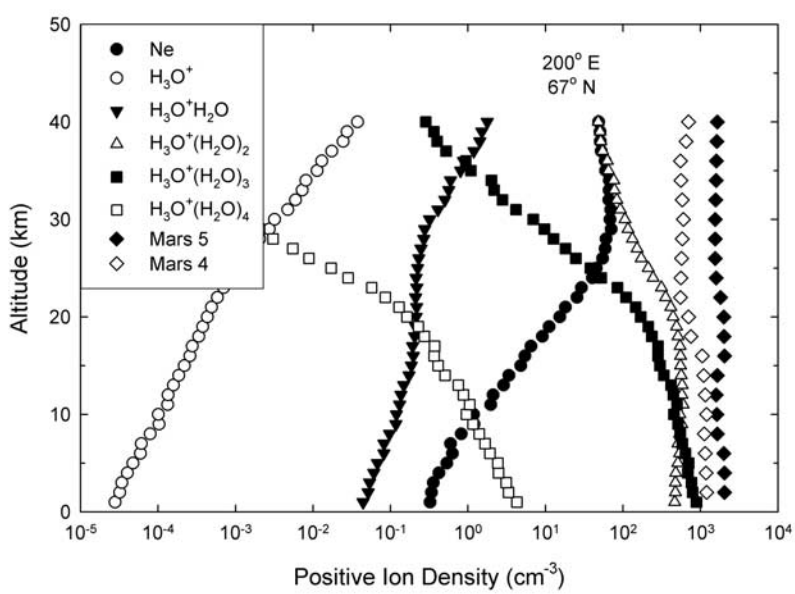

Figure 4a. Altitude profiles of positive ion densities in the Martian troposphere at latitude 67°N and longitude 200°E due to precipitation of galactic cosmic rays at solar zenith angle 80°.

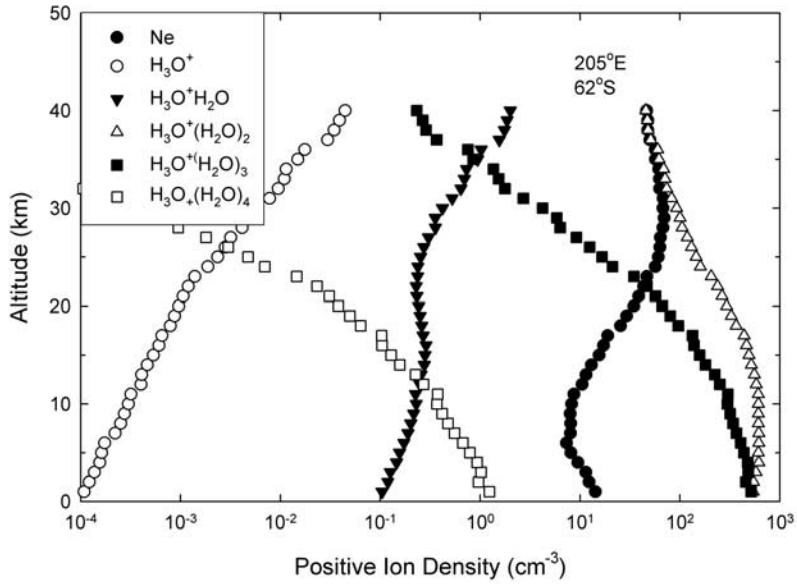

Figure 4b. Altitude profiles of positive ion densities in the Martian troposphere at latitude 62°S and longitude 205°E due to precipitation of galactic cosmic rays at solar zenith angles 85°.

and 18 February 1974 [*Savich and Samovol*, 1976]. These observations were carried out by radio occultation experiment in spring season at coordinate 38°N 214°W and local time 0430 with solar zenith angle 106° during low solar activity period. In Figure 4a the calculated electron density is compared with these measurements. Each measured profiles show existence of plasma at height below 40 km with a small shoulder of electron density between $\sim 10^3$ cm^{-3} and 2×10^3 cm^{-3} at altitude $\sim$ 20 km. This signature is not very prominent and other published Mars low altitude profiles do not show similar features [*Zhang et al.*, 1990]. There has been found that calculated electron density is smaller from the measurements by an order of magnitude around the peak altitude. This difference increases up to $\sim$3 order of magnitude near the surface of Mars. Our low values of electron density may arise because of several reasons: (1) If the measured electron density on 10 and 18 February 1974 is caused by high cosmic ray fluxes, it should have high values from the estimated electron density. The present calculation is made using galactic cosmic ray population of fluxes 10^3 to 10^{-5} particle m^{-2} s^{-1} GeV^{-1} $ster^{-1}$ for energy range 1–1000 GeV. We do not know how much flux of galactic cosmic rays actually precipitate in the daytime/nighttime atmosphere of Mars. (2) There is a large error in the measurements. The presence of plasma in the lower ionosphere is derived on the basis of formal inversion of the set of observations in symmetrical approximation. During the occultation measurements, the possible displacement of electron density due to this error was estimated to be $\sim\pm 500$ cm^{-3} [*Savich and Samovol*, 1976]. This could be an important reason for the difference between calculation and measurement at low ionospheric region. (3) Because of the large uncertainty in the measurements, ion and electron density could not separate out. If it is true, the calculated total (ion + electron) density can be brought into close agreement with the measurements. (4) Mars 4/5 have observed plasma density at low solar activity period. The flux of cosmic radiation is correlated with the solar activity through the solar wind, which decelerates the low energy cosmic particles in the interplanetary medium. During the period of low solar activity the cosmic rays' ionization and plasma density become higher. (5) Finally, A global dust storm could also enhance the measured plasma density due to heating effect in the Martian troposphere [cf. *Bougher et al.*, 1999]. The ground-based observations have reported that Mars was covered by dust storms at most of the time of radio measurements carried by Mars 4/5 in 1974 [*Martin*, 1975; *Dollfus et al.*, 1984].

[22] The number densities of five major negative ions (CO_4^-, CO_3^-, $CO_3^-H_2O$, $CO_3^-(H_2O)_2$, and $NO_2^-H_2O$) are shown in Figures 5a and 5b for the same locations as shown in Figures 4a and 4b. Water cluster of CO_3^- and NO_2^- (i.e., $CO_3^-(H_2O)_n$, $NO_2^-(H_2O)_n$ for n = 1 and 2) are dominant ions below 30 km. Above this altitude electron plays an important role in the lower ionosphere of Mars. The electron density is plotted in both figures. The relative high abundance of oxygen bearing molecules permits the presence of negative ions in the lower ionosphere. Initially, negative ions O^- and O_2^- are produced through electron capture by ozone and molecular oxygen, respectively, as given below:

$$e + O_3 \rightarrow O^- + O_2 \quad \text{(R7)}$$

$$e + O_2 + M \rightarrow O_2^- + h\nu \quad \text{(R8)}$$

Later CO_3^- and CO_4^- are produced from three body reactions as:

$$O^- + CO_2 + M \rightarrow CO_3^- + M \quad \text{(R9)}$$

$$O_2^- + CO_2 + M \rightarrow CO_4^- + M \quad \text{(R10)}$$

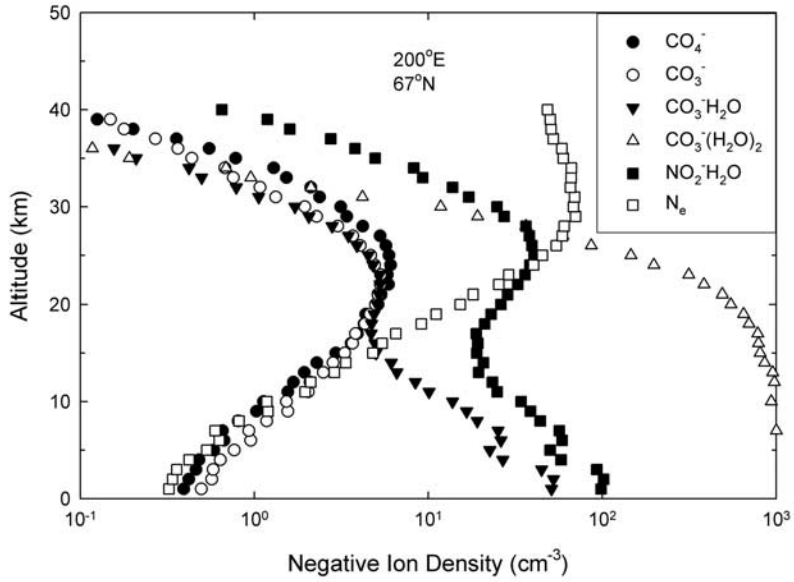

Figure 5a. Altitude profiles of negative ion densities in the Martian troposphere at latitude 67°N and longitude 200°E due to precipitation of galactic cosmic rays at solar zenith angle 80°.

The ion CO_4^- is destroyed by atomic oxygen producing CO_3^-, whose peak occurs at about 25 km. The loss of CO_3^- with H_2O is the major source of production of $CO_3^-H_2O$ and $CO_3^-(H_2O)_2$ as given below:

(R11) $$CO_3^- + H_2O + M \leftrightarrow CO_3^-H_2O + M$$

(R12) $$CO_3^-H_2O + H_2O + M \leftrightarrow CO_3^-(H_2O)_2 + M$$

These reactions produce 100% $CO_3^-(H_2O)_2$ at all heights in the troposphere of Mars. The ion CO_3^- is also destroyed by NO forming NO_2^- ion. Later NO_2^- was hydrated by three body reaction with water vapor producing second important ions $NO_2^-(H_2O)_n$ for n = 1 and 2 as:

(R13) $$CO_3^- + NO \rightarrow NO_2^- + CO_2$$

(R14) $$NO_2^- + H_2O + M \leftrightarrow NO_2^-H_2O + M$$

(R15) $$NO_2^-H_2O + H_2O + M \leftrightarrow NO_2^-(H_2O)_2 + M$$

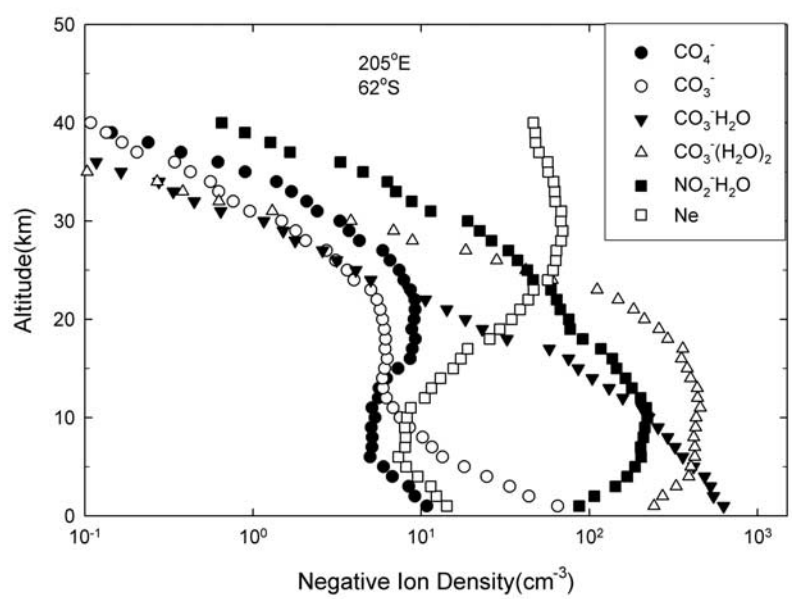

Figure 5b. Altitude profiles of negative ion densities in the Martian troposphere at latitude 62°S and longitude 205°E due to precipitation of galactic cosmic rays at solar zenith angles 85°.

Table 1. Chemical Reactions

$O_4^+ + h\nu$ ($\lambda \sim 6000-9000$ Å) $\rightarrow O_2^+ + O_2$	0.13	*Totmatsu* [1990]
$O_2^+H_2O + h\nu$ ($\lambda \leq 6000$ Å) $\rightarrow O_2^+ + H$	0.18	*Totmatsu* [1990]
$O_2^+(H_2O)_2 + h\nu$ ($\lambda \leq 6000$ Å) $\rightarrow$ Products	0.27	*Totmatsu* [1990]
$CO^- + h\nu$ ($\lambda \sim 6000$ Å) $\rightarrow e + CO$	0.01	*Whitten et al.* [1971]
$CO_3^- + h\nu$ ($\lambda < 6800$ Å) $\rightarrow e + CO_3$	0.0098	*Turunen et al.* [1996]
$CO_3^- + h\nu$ ($\lambda < 6800$ Å) $\rightarrow O^- + CO_2$	0.076	*Turunen et al.* [1996]
$CO_3^-H_2O + h\nu$ ($\lambda < 7000$ Å) $\rightarrow CO_3^- + H_2O$	0.27	*Fritzenwallner and Kopp* [1998]
$CO_3^-(H_2O)_2 + h\nu$ ($\lambda < 6900$ Å) $\rightarrow CO_3^- + H_2O + H_2O$	0.27	*Molina-Cuberos et al.* [2002]
$CO_4^- + h\nu$ ($\lambda \leq 3500$ Å) $\rightarrow O_2^- + CO$	0.0028	*Turunen et al.* [1996]
$NO_2^- + h\nu$ ($\lambda < 5200$ Å) $\rightarrow e + N$	0.018	*Totmatsu* [1990]
$NO_3^- + h\nu$ ($\lambda < 3200$ Å) $\rightarrow e + NO + O_2$	0.002	*Swider* [1996]
$NO_3^- + h\nu$ ($\lambda < 3200$ Å) $\rightarrow NO_2^- + O$	0.026	*Swider* [1996]
$O^- + h\nu$ ($\lambda < 8500$ Å) $\rightarrow e + O$	0.62	*Turunen et al.* [1996]
$O_2^- + h\nu$ ($\lambda \leq 8500$ Å) $\rightarrow e + O_2$	0.17	*Turunen et al.* [1996]
$O_3^- + h\nu$ ($\lambda < 5900$ Å) $\rightarrow e + O_3$	0.021	*Turunen et al.* [1996]
$O_3^- + h\nu$ ($\lambda < 5900$ Å) $\rightarrow O^- + O_2$	0.21	*Turunen et al.* [1996]

(R6), (R11), (R12), (R14), and (R15) are reversible reactions. Near the surface, the densities of negative ions and electron are reduced by about an order of magnitude in northern summer than that of southern winter. The position of the ionization peak is also varying between these two seasons. In summer the ionization peaks are found at altitude $\sim$25 km for ions $CO_3^-H_2O$, CO_3^- and CO_4^- and for ion $NO_2^-H_2O$ at altitude 28 km. In winter the maximum ionizations for ions CO_3^-/CO_4^- and $NO_2^-H_2O$ occur at altitude $\sim$20 km and 7 km, respectively. The ions $CO_3^-H_2O$ and $CO_3^-(H_2O)_2$ do not represent clear ionization peaks in southern and northern seasons, respectively. In this model calculation we have used ion-neutral, electron neutral, photo dissociation of positive and negative ions, electron photo-detachment, ion-ion, ion-electron recombination processes through over 133 chemical reactions. Three body reactions are very important at Mars, but most of them have been measured using N_2 or O_2 as a third body and the rate coefficient with CO_2 is unknown. When no rate coefficient for CO_2 is available, we have used the known data as valid for Mars' atmosphere conditions. However the rate coefficient does not depend too much on third body. It is known that three body reaction rate coefficient asymptotically approach a limit at high pressure and that the high pressure behavior of such reactions is similar to bimolecular processes. The density of Martian atmosphere is not high enough to saturate the trimolecular reactions included in this model and no limit in the effective bimolecular rate was used here. The chemical reactions are taken from *Haider et al.* [2007]. They have not used photodissociation and electron photo-detachment reactions, which occur in the daytime troposphere. These reactions are given in Table 1. The units of these reactions are s^{-1}. Their rate coefficients are calculated from known values of the terrestrial atmosphere and divided by 2.25 to account for the reduced solar radiation at Mars compared with that on earth. The solar flux on Mars is scaled by $1/R^2$ where R is the heliocentric distance equal to 1.5 AU. The photodissociation of CO_3^-, CO_4^-, and NO_3^- leads to initial values of oxygen and nitric anions, respectively. The electron photodetachment of negative ions are not found very important process between altitudes 0 and 10 km. Above this height photodetachment of CO_3^-/CO_4^- plays a significant role for the production of electron density. The transport of molecular ions is not considered in this model calculation because the transport time is several orders of magnitude higher than the chemical life time.

[23] In comparing dayside ion density with our nightside calculation [*Haider et al.*, 2007], we find that densities of daytime hydronium ions ($H_3O^+(H_2O)_n$ for n = 1, 2, 3, and 4) are lower from the nighttime by a factor of $\sim$2. The negative ion densities of water clusters of NO_2^- and CO_3^-(i.e., $NO_2^-(H_2O)_n$ and $CO_3^-(H_2O)_n$ for n = 1, 2) are more structured in the dayside ionosphere as compared to that of nighttime. The difference between daytime and nighttime ion densities is due to different model atmospheres used in both model calculations. The chemistry of the negative ions is very sensitive to the neutral density. Therefore, more variations are found on the densities of negative ions as compared to the positive ions.

[24] D layer is observed in the lower ionosphere of earth at 65–70 km because of the precipitation of galactic cosmic rays. The mean atmospheric pressure of Mars is nearly 1000 times less than that on earth (The atmospheric pressures on Mars and earth are nearly 6 mb and 1000 mb, respectively). Therefore, galactic cosmic rays penetrate deeper into the Martian atmosphere as compared to that on earth's atmosphere. By analogy to earth's ionosphere, we suggest that Martian ionosphere consists D layer in the troposphere. The position and value of this layer are different in summer and winter seasons at high northern and southern latitudes, respectively. In the dayside ionosphere, we have neither in situ measurements of low altitude ion layers nor remote sensing measurements from Mars surface. The direct measurements of cluster ions and electron density in the lower ionosphere of Mars can be performed by Sounding rocket and Langmuir probe experiments onboard Mars Lander, respectively. Sounding rockets carrying quadrupole ion mass spectrometer has been found very useful experiment to measure positive and negative ion densities in the D region of Earth's ionosphere. Langmuir probe has been used in rockets and balloons to measure electron density in the lower ionosphere of Earth. Ground-based remote sensing experiments such as ionosondes and Incoherent Scatter Radars are routinely used to measure D layer on Earth. These two experiments can also be performed on Mars from a ground-based laboratory.

5. Conclusions

[25] We have analyzed MGS/radio science data in the Martian troposphere at high latitudes 67°N and 62°S and

longitudes 200°E and 205°E, respectively. These data sets were observed in northern summer (Ls = 67°) and southern winter (Ls = 285°) at solar zenith angles 80° and 85°, respectively. At the time of these measurements, Mars had moderate solar activity period ($f_{10.7}$ = 132–181). We have used these data in the calculation of production rate, positive ion density, negative ion density, and electron density. The calculations are made under photochemical steady state condition using energy loss model and continuity equation. The calculated electron density is compared with nighttime observations made by Mars 4 and 5. The impact ionization source is taken as galactic cosmic rays with the population of fluxes 10^3 to 10^{-5} particles m^{-2} s^{-1} GeV^{-1} $ster^{-1}$ for energy range 1–1000 GeV [*Haider et al.*, 2007]. We do not know what fraction of galactic cosmic rays actually precipitate at high northern and southern latitudes during summer and winter seasons. Therefore, we have used same energy flux of galactic cosmic rays in both calculations. The hydrated hydronium ions ($H_3O^+(H_2O)_n$ for n = 1, 2, 3, and 4) and water cluster of NO_2^- and CO_3^- (i.e., $NO_2^-(H_2O)_n$ and $CO_3^-(H_2O)_n$ for n = 1, 2) are dominated in the Martian troposphere. The maximum electron densities in southern winter and northern summer are obtained at altitudes ~25 km and ~30 km with the concentrations ~70 cm^{-3} and ~80 cm^{-3}, respectively, because of the high efficiency of electron attachment to O_x molecules. The positive/negative ion densities are changed by factors of 5 to 10 between these two seasons due to use of different model atmospheres.

[26] **Acknowledgments.** Authors are thankful to G. L. Tyler, Stanford University Stanford, California, USA, for his encouragement and providing us radio science data through the website (http://pds-geophys.wustl.edu/pds/mgs/rs/).

[27] Amitava Bhattacharjee thanks Anil Bhardwaj and Thomas Cravens for their assistance in evaluating this paper.

References

Anderson, D. E., and C. W. Hord (1971), Mariner 6 and 7 ultraviolet spectrometer experiment: analysis of hydrogen Lyman alpha data, *J. Geophys. Res.*, *76*, 6666–6673.

Barker, E. S. (1972), Detection of molecular oxygen in the Martian atmosphere, *Nature*, *238*, 447–448.

Barth, C. A., and C. W. Hord (1971), Mariner ultraviolet spectrometer: Topography and polar cap, *Science*, *173*, 197–201.

Barth, C. A., W. Hord, A. I. Stewart, A. L. Lane, M. L. Dick, and G. P. Anderson (1973), Mariner 9 ultraviolet spectrometer experiment: Seasonal variations of ozone on Mars, *Science*, *179*, 795–796.

Biemann, K., T. Owen, D. R. Rushneck, A. L. lafleur, and D. W. Howarth (1976), The atmosphere of Mars near the surface: Isotope ratios and upper limits on noble gases, *Science*, *194*, 76–78.

Bougher, S. W., S. Engel, R. G. Roble, and B. Foster (1999), Comparative terrestrial planet thermosphere, 2, solar cycle variation of global structure and winds at equnox, *J. Geophys. Res.*, *104*, 16,591–16,611.

Carleton, N. P., and W. A. Traub (1972), Detection of molecular oxygen on Mars, *Science*, *177*, 988–992.

Dalgarno, A., and M. B. McElroy (1970), Mars: Is nitrogen present?, *Science*, *170*, 167–168.

Dollfus, A., E. Bowell, and S. E. Bisawa (1984), The Martian dust storms of 1973: Apolarimetric analysis, *Astron. Astrophys.*, *134*, 343.

Evans, R. D. (1955), The atomic nucleus, McGraw Hill Publication, USA, pp. 567–591.

Fritzenwallner, J., and E. Kopp (1998), Model calculations of negative ion chemistry in the mesosphere with special emphasis on the chlorine species and the formation of cluster ions, *Adv. Space Res.*, *21*(6), 894.

Grandjean, J., and R. M. Goody (1955), The concentration of carbon dioxide in the atmosphere of Mars, *Astrophys. J.*, *121*, 548–552.

Haider, S. A., S. P. Seth, E. Kallio, and K. I. Oyama (2002), Solar UEV and electron-proton-hydrogen atom produced ionosphere on Mars: Comparative studies of partice fluxes and ion production rates due to different processes, *Icarus*, *159*, 18–30.

Haider, S. A., V. Singh, V. R. Choksi, W. C. Maguire, and M. I. Verigin (2007), Calculated densities of $H_3O+(H_2O)_n$, $NO_2-(H_2O)_n$,$CO_3-(H_2O)_n$ and electron in the nighttime ionosphere of Mars: Impact of solar wind electron and galactic cosmic rays, *J. Geophys. Res.*, *112*, A12309, doi:10.1029/2007JA012530.

Istomin, V. G., and K. V. Grechnev (1976), Argon in the Martian atmosphere: Evidence from the Mars 6 descent module, *Icarus*, *28*, 155–158.

Kaplan, L. D., G. Munch, and H. Spinard (1964), An analysis of the spectrum of Mars, *Astrophys. J.*, *139*, 1–15.

Kaplan, L. D., J. Connes, and P. Connes (1969), Carbon monoxide in the Martian atmosphere, *Astrophys. J.*, *157*, L187–L192.

Kliore, A. J., D. L. Cane, G. S. Levy, V. R. Eshleman, G. Fjeldbo, and F. D. Drake (1965), Occultation experiment: Results of the first direct measurement of Mars' atmosphere and ionosphere, *Science*, *149*, 1243–1248.

Kuiper, G. P. (Ed.) (1952), *The Atmosphere of Earth and Planets*, Chapter XII.

Martin, L. J. (1975), North polar hood observations during Martian dust storms, *Icarus*, *6*, 341.

McElroy, M. B., Y. L. Yung, and A. O. Neir (1976), Isotopic composition of nitrogen: Implications for the past history of Mars atmosphere, *Science*, *194*, 70–72.

Michael, M., M. Barani, and S. N. Tripathi (2007), Numerical predictions of aerosol charging and electrical conductivity of the lower atmosphere of Mars, *Geophys. Res. Lett.*, *34*, L04201, doi:10.1029/2006GL028434.

Molina-Cuberos, G. J., H. Lichtenegger, K. Schwingenschuh, J. J. Lopez-Moreno, and R. Rodrigo (2002), Ion neutral chemistry model of the lower ionosphere of Mars, *J. Geophys. Res.*, *107*(E5), 5027, doi:10.1029/2000JE001447.

Montmessin, F., E. Quemerais, J. L. Bertaux, O. Korablev, P. Rannou, and S. Lebonnois (2006), Stellar occultations at UV wavelengths by the SPICAM instrument: Retrieval and analysis of Martian haze profiles, *J. Geophys. Res.*, *111*, E09S09, doi:10.1029/2005JE002662.

Nier, A. O., W. B. Hanson, A. Seif, M. B. Mcelroy, N. W. Spencer, R. J. Duckett, T. C. D. Knight, and W. S. Cook (1976), Composition and structure of the Martian atmosphere: Preliminary results from Viking 1, *Science*, *193*, 786–788.

Nair, H., M. Allen, A. D. Anbar, Y. L. Yung, and R. T. Clancy (1994), A photochemical model of the Martian atmosphere, *Icarus*, *111*, 124–150.

O'Brien, K., K. W. Friedberg, H. H. Sauer, and D. F. Smart (1996), Atmospheric cosmic rays and solar energetic particles at aircraft altitudes, *Environ. Int.*, *22*, S9–S44, Suppl. 1.

Owen, T., and K. Biemann (1976), Composition of the atmosphere at the surface of Mars: Detection of Argon-36 and preliminary analysis, *Science*, *193*, 801–803.

Owen, T., K. Biemann, D. R. Rushneck, J. E. Biller, D. W. Howarth, and A. L. Lafleur (1976), The atmosphere of Mars: Detection of Krypton and Xenon, *Science*, *194*, 1293–1295.

Owen, T., K. Biemann, D. R. Rushneck, J. E. Biller, D. W. Howarth, and A. L. Lafleur (1977), The composition of the atmosphere at the surface of Mars, *J. Geophys. Res.*, *82*, 4635–4644.

Rodrigo, R., E. Gracia-Alvarez, M. J. Lopez-Gonzalez, and J. J. Lopez-Moreno (1990), A non-steady one dimensional theoretical model of Mars' neutral atmospheric composition between 30 and 200 km, *J. Geophys. Res.*, *95*, 14,975–14,810.

Savich, N. A., and V. A. Samovol (1976), The night time ionosphere of Mars from Mars 4 and Mars 5 dual frequency radio occultation measurements, *Space Res.*, *XVI*, 1009–1010.

Spinrad, H., G. Munch, and L. D. Kaplan (1963), The detection of water vapor on Mars, *Astrophys. J.*, *137*, 1319–1321.

Strickland, D. J., G. E. Thomas, and P. R. Sparks (1972), Mariner 6 and 7 ultraviolet spectrometer experiment: Analysis of the OI 1304A and 1356A emissions, *J. Geophys. Res.*, *77*, 4052–4068.

Swider, W. (1996), Steady state D region model, in *Solar Terrestrial Energy Program: Handbook of Ionospheric Model*, edited by R. W. Schunk, 27–32.

Totmatsu, T. (1990), Compendium of Aeronomy, Terra Scientific Publishing Company, Tokyo, Japan, 195–257.

Turunen, E., H. Matveinen, J. Tolvanen, and H. Ranta (1996), D region ion chemistry model, in *Solar Terrestrial Energy Program: Handbook of Ionospheric Models*, edited by R. W. Schunk, 1–25.

Tyler, G. L., G. Balmino, D. P. Hinson, W. S. Sjogren, D. E. Smith, R. A. Simpson, S. W. Asmar, P. Priest, and J. D. Twicken (2001), Radio science observations with Mars Global Surveyor: Orbit insertion through one Mars year in mapping orbit, *J. Geophys. Res.*, *106*, 23,327–23,348.

Whitten, R. C., I. G. Poppoff, and J. S. Sims (1971), The ionosphere of Mars below 80 km altitude, 1, *Planet. Space Sci.*, *17*, 243–250.

Young, L. D. G., and A. T. Young (1977), Interpretation of high resolution spectra of Mars IV. New calculations of CO abundance, *Icarus*, *30*, 75–79.

Zhang, M. H. G., J. G. Luhmann, and A. J. Kliore (1990), An observational study of the night side ionosphere of Mars and Venus with radio occultation methods, *J. Geophys. Res.*, *95*, 17,095–17,107.

S. A. Haider and V. Sheel, Department of Space and Atmospheric Sciences, Physical Research Laboratory, Navrangpura, Ahmedabad 380 009, India. (haider@prl.res.in)

W. C. Maguire, Solar System Exploration Division, NASA Goddard Space Flight Centre, Mail Code 693, Greenbelt, MD 20771, USA.

G. J. Molina-Cuberos, Fac. Quimica, Campus de Espinardo, Universidad de Murcia, E30100 Murcia, Spain.

V. Singh, Department of Electronics for Automation, Faculty of Engineering, University of Brescia, Via Branze 38-25123 Brescia, Italy.